BULLETIN OF THE EARTHQUAKE
RESEARCH INSTITUTE
UNIVERSITY OF TOKYO
Vol. 65 (1990) pp. 1-32

Depth Extent Analysis of the 1981 October 16 Chile Earthquake

Tetsuzo SENO[1] and Satoru HONDA[2]

[1]Earthquake Research Institute
[2]Institute of Geology and Mineralogy, Faculty of Science,
Hiroshima University

(Received December 28, 1989)

Abstract

We present a method to retrieve the vertical rupture extent of a large shallow earthquake whose rupture mode is assumed to be simple. In this method, we calculate GREEN's functions of vertically distributed point sources which mimic upward or downward rupture propagation with a constant velocity. Using these GREEN's functions we deconvolve P-wave data to obtain source time functions for the assumed depth extent and rupture direction. First we estimate the maximum source duration for point sources by letting the length of the source time function be as long as that of the data. We then deconvolve the source time function limiting its maximum length to be shorter than the time window of the data but long enough to cover the maximum duration for the point sources. We take the depth extent and rupture direction which gives the minimum residual as the optimum solution.

We test this method by deconvolving the synthetic data using kernels slightly different from those used for the synthetics. We find that the deconvolution is robust to the rupture velocity. However, the crustal structure near the source, in particular a water layer thickness different from that used for the synthetics, has a significant effect on the deconvolution. The deconvolution is moderately sensitive to the focal mechanism.

We applied this method to a large outer-rise (M_S=7.2) earthquake which occurred west of the Chile Trench on October 16, 1981. We determined the water layer thickness to be 4.5 km, which gives the smallest residuals. We obtained a 30 or 40 km deep point source as an optimum for this event, using 10 km grid spacing, i.e., a 10 km depth interval between point sources. Using 5 km grid spacing, we obtained a rupture from 37 to 32 km depth; however, the difference

between the residuals for different rupture modes is so small that this rupture extent does not seem meaningful.

In order to obtain more information on the depth extent of this event, we conducted further synthetic data/deconvolution experiments. In the calculation of synthetics, we restricted the shape of the source time function to be an isosceles triangle, whose width is determined by matching the total source duration observed for point sources at 20–40 km depth. We compared the source time functions deconvolved from the synthesized data with those obtained from the observed data. To explain the observed source time functions and residual patterns, a centroid depth at 35 km and depth extent less than 15 km are required. Upward rupture propagation is preferred. We consider the solution with rupture from 41 to 29 km (12 km depth extent with a centroid at 35 km) to be the optimum solution for the 1981 Chile earthquake.

This depth extent coincides with the lower half of the mechanical plate of 40 Ma age, which is the age of the ocean floor at the epicenter, and is consistent with the compressional stress in the deeper portion of the plate associated with its bending prior to subduction beneath the Chilean coast.

1. Introduction

It is important to know accurate source depths of intraplate earthquakes in order to clarify their tectonic significance and the stress state of the lithosphere. For small earthquakes, we may constrain their focal depths by a comparison of observed long-period P-waveforms with synthesized seismograms (e. g., STEIN and WIENS, 1986). However, when earthquakes become large, this forward modeling approach does not work well because of the well-known trade-off between the source depth and the source time function (CHRISTENSEN and RUFF, 1985; STEIN and WIENS, 1986), since the arrival time differences between P and depth phases (pP, sP, pwP, pwwP and so on) become comparable to the source duration.

A few methods have been so far proposed to overcome this difficulty. In one method, source time functions deconvolved at several assumed depths are compared and the depth or depth range where the deconvolution gives simpler source time function is taken as the depth or depth range of the fault (FORSYTH, 1982; CHRISTENSEN and RUFF, 1985). In another method, we deconvolve data at multiple stations, and take the depth where it gives the smallest residual as the centroid depth (STEIN and WIENS, 1986). However, both methods have the intrinsic difficulty that the GREEN's

function for an extended source may be significantly different from that of a point source, when the earthquake is large. For example, STEIN and WIENS (1986) showed that for a depth extent larger than 30 km, the waveform may be skewed significantly due to its rupture propagation.

In this paper we present a method to retrieve the depth extent of large earthquakes from long-period P-waves; in this method we deconvolve the data to obtain a source time function using GREEN's functions from vertically extended point sources which propagate upward or downward with a constant velocity. By synthetic data experiments, we examine the effects of the assumed rupture velocity, crustal structure and focal mechanism on the deconvolution. We find that the crustal structure affects severely, and the focal mechanism affects moderately, the results of the deconvolution. We have to take these effects into account to retrieve the depth extent correctly.

We apply this method to the Chile earthquake of October 16, 1981 (M_S=7.2) which occurred within the Nazca plate at the outer-rise off the Chile Trench (Fig. 1a). The source parameters of this event determined by CHRISTENSEN and RUFF (1985) and HONDA and SENO (1989) are listed in Table 1. Fig. 1b shows the mechanism diagram of these solutions with

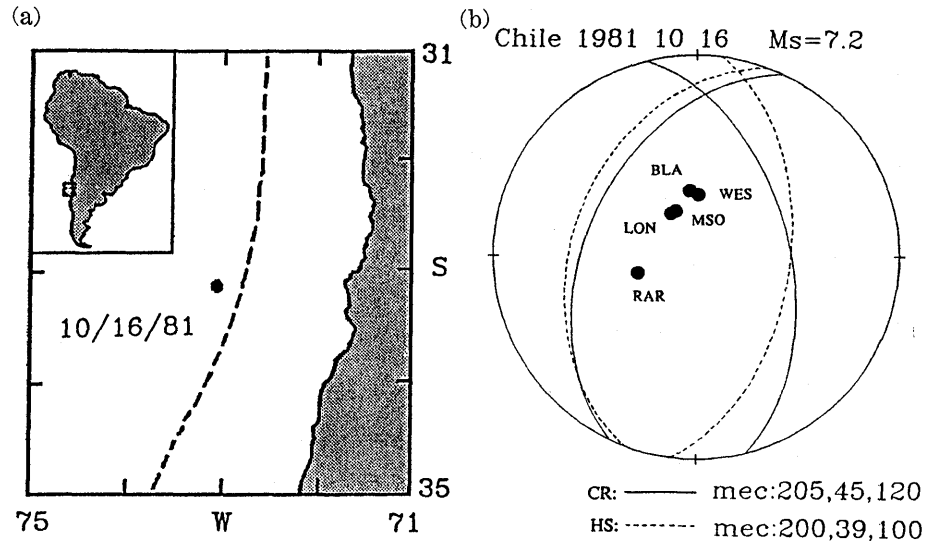

Fig. 1. (a) Epicenter of the 1981 October 16 Chile earthquake (HONDA *et al.*, 1990). (b) Focal mechanism solution of the Chile earthquake. Nodal lines of P-wave first motions are plotted in the lower hemisphere of the focal sphere using equal area projection. CR (solid line) denotes the solution by CHRISTENSEN and RUFF (1985) and HS (dotted line) by HONDA and SENO (1989). The stations used in this paper are plotted along with their P-wave first motions. The strike, dip and slip angles are shown at the bottom.

Table 1. Hypocentral and source parameters of the Chile earthquake

Origin time	Epicenter	m_b	M_S	Mechanism Solution ϕ	δ	λ
16 October 1981	33.15S	6.2	7.2	CR: 205	45	120
10 h 25 min 40 s	73.10W			HS: 200	39	100

Hypocentral parameters are from ISC Bulletin. ϕ, δ and λ are the strike, dip and slip angles of the fault plane solution. CR is from CHRISTENSEN and RUFF (1985) and HS is from HONDA and SENO (1989).

the stations used for the present analysis. These solutions represent an E-W horizontal compression.

CHRISTENSEN and RUFFF (1985) and WARD (1983) obtained the depth ranges of 5-25 km and 12-24 km, respectively, for this event. These results suggest that the compressional stress in this area may be above the neutral plane of the bending stress within the plate, which in turn implies that the tectonic stress, which originates from the combination of ridge push, interplate seismic coupling at the thrust zone and slab pull, has the same order of magnitude as the bending stress. Since tectonic stresses are on the order of several hundred bars—1 kilobar (LISTER, 1975; PARSONS and RICHTER, 1980; DAVIES, 1983; WIENS and STEIN, 1985; FROIDEVAUX *et al.*, 1988), this further implies that the bending stress is on the order of at most 1 kbar. On the contrary, HONDA and SENO (1989) and HONDA *et al.* (1990) obtained a centroid depth for this event between 20 and 45 km, which suggests a deeper source than those obtained previously.

However, in order to discuss the perturbation of the neutral plane, we have to determine the vertical rupture extent of this event precisely, rather than to know only its centroid depth. In this study we try to retrieve the depth extent of this event by applying the above method. We obtained a rupture from 41 to 29 km as the optimal solution, which indicates that the faulting is just below the neutral plane, that can be expected from the bending of a plate of this age. This suggests that the stress perturbation due to tectonic stresses, if it exits, is small compared with the bending stress in this region.

A brief description of the method and part of the results of the analysis of the Chile earthquake have been presented by HONDA *et al.* (1990).

2. Deconvolution

The seismogram $y(t)$ generated from a point double-couple source and recorded at teleseismic distance can be written as

$$y(t)=S(t)*g(t)\,, \tag{1}$$

where $S(t)$ is the far-field source time function, which represents the moment release rate, and $g(t)$ is the GREEN's function, that is, the transfer function of the earth and the instrument. The GREEN's function $g(t)$ is given by

$$g(t)=\frac{g_S c_0}{4\pi\rho\alpha^3 a_0}R(t)*Q(t)*I(t) \tag{2}$$

(KANAMORI and STEWART, 1976), where g_S and c_0 are the ray geometric spreading and free-surface receiver factors, α and ρ are the P-wave velocity and density at the source, a_0 is the radius of the earth, and $R(t)$, $Q(t)$ and $I(t)$ are the pulses of rays, instrument and attenuation impulse responses, respectively. $R(t)$ can be expressed as follows,

$$R(t)=\sum_x R_x r_x \delta(t-t_x) \tag{3}$$

where, R_x is the radiation pattern factor for the x-th phase (P, pP, sP, pwP, etc.), r_x is the wave conversion factor for phase x, and t_x is the travel time delay relative to P.

We sum up $g(t)$ for point sources vertically distributed with equal grid spacing by taking into account the phase delays due to rupture propagation and vertical slowness. Each source is assumed to have the same double-couple focal mechanism and an equal displacement time history, assuming that the horizontal rupture is uniform over each point source. $R(t)*Q(t)*I(t)$ from a point source is calculated by the code written by KROEGER and GELLER (1983), in which all the effective rays reflected or converted from a layered crust can be taken into account. For the attenuation operator $Q(t)$ (CARPENTER, 1966), $t_p{}^*=1$ sec is assumed. The geometrical spreading factor is calculated from HERRIN's (1968) travel time table, assuming $\alpha=6.0$ km/sec and $\rho=2.7$ gr/cm^3 at the receiver. C_0 is set to be 2.0.

The source time function $S(t)$ is represented by a series of isosceles triangles; the latter half of the bottom of each triangle is overlapped with the former half of the next triangle. Then the source time function $S(t)$ may be written,

$$S(t)=\sum_i m_i s(t-(i-1)\Delta t)\,, \tag{4}$$

where $s(t)$ represents a unit isosceles triangle function with a bottom

length of $2\Delta t$. The residual normalized by the data variance is defined by

$$\text{res.}=\int_0^T[x_{\text{obs}}(t)-x_{\text{syn}}(t)]^2dt\Big/\int_0^T[x_{\text{obs}}(t)]^2dt \qquad (5)$$

We obtain a set of m_i which minimizes the residual by a conventional least squares method. A set of normal equations are,

$$d_i=G_{ij}m_j \qquad (6)$$

where d_i is the data at time t_i, and $G_{ij}=g(t)*s(t-(j-1)\Delta t)|_{t=t_i}$.

3. Test of the Method

3.1 General procedure

We generate synthetic data using the crustal structure denoted by C1 in Table 2 and the mechanism solutions of the October 10, 1981 Chile earthquake by CHRISTENSEN and RUFF (1985) and HONDA and SENO (1989) (Table 1; hereafter these solutions are denoted by CR and HS, respectively). GREEN's functions are calculated and summed up over the point sources assuming a rupture velocity of 3 km/sec. It is then convolved with a trapezoidal source time function with a width of 3, 3 and 3 sec. (This function is denoted by (3, 3, 3) hereafter).

We first deconvolve the synthetic data by GREEN's functions for various rupture extents using a time span allowed for the source time function as long as that of the data time window. We call this *long time deconvolution* in this paper. The bottom length of the unit triangle of the source time function, i.e. $2\Delta t$, is set to be 6 sec. Sampling rate and data length are 1 Hz and 60 sec, respectively. In the long time deconvolution, the latest part of the solutions, m_i, becomes unstable because of lack of data to constrain these parameters (RUFF and KANAMORI, 1983).

Table 2. Crustal structure used in the calculation of GREEN's functions.

C1	V_P (km/sec)	V_S (km/sec)	ρ (gr/cm^3)	thickness (km)
	1.0	0.0	1.03	4.5
	2.0	1.15	1.90	1.0
	4.7	2.71	2.40	1.6
	6.6	3.81	2.80	4.5
	8.1	4.68	3.30	
C2	V_P (km/sec)	V_S (km/sec)	ρ (gr/cm^3)	thickness (km)
	1.0	0.0	1.03	4.5
	6.6	3.81	2.80	

We use a damped least squares method in this case; the damping factor, defined as a fraction of the largest diagonal component of the matrix G^tG, is set to be 0.01.

Fig. 2a shows the deconvolved source time functions at WES; the synthetic seismogram generated over 27 km to 42 km point sources distributed at every 3 km depth using solution CR is deconvolved by the GREEN's functions generated by the same solution using point sources distributed at every 10 km depth. This deconvolution is denoted by CR/CR and 27-42(3)/xx-yy(10), writing the parameter used in the synthetics before that used in the GREEN's function. The abscissa in Fig. 2a indicates the starting depth xx and the ordinate the final depth yy of the point sources used in the kernel. The numerals beneath each source time function represent the normalized residual (eqn. 5) multiplied by 1000. The differences from the minimum residual, which is shown at the bottom, are shown. We use the notation xx-yy for the solution deconvolved by the kernel which starts at xx km depth and stops at yy km depth.

As we can see from this figure, the minimum residual appears at 30-40 as expected. However, other depth ranges also give residuals less than 1% (i.e., less than 10) of the data variance. This is because the time length of the source time function is allowed to be long enough to fit the data equally well for the wide range of depth extents used in the deconvolution. Therefore it is not effective to use the minimum residual to select the optimal solution in this case.

For such a case, CHRISTENSEN and RUFF (1985) proposed to take the depth range over which point sources give a simple source time function as the depth extent of the rupture. It appears that this simplicity criterion holds in Fig. 2a, where 30 and 40 km point sources (i.e., 30-30 and 40-40) give simple source time functions. However, this is fortuitous. Fig. 2b shows the results of deconvolution of HS/HS, and 41-29(3)/xx-yy(10). In this case, simple source time functions appear at the point sources from 20-20 to 40-40. Therefore, in this study we do not use the simplicity criterion; instead we perform a *short time deconvolution* as described below.

From the long time deconvolution above we can estimate the source duration for each depth extent. Noting that the source time needed for distributed sources is shorter than those for a point source, we can obtain an estimate for the maximum source duration needed to describe the source. In the short time deconvolution, we constrain the maximum time span of the source time function to be longer than the source duration, but shorter than the data time window. The deconvolution results do not

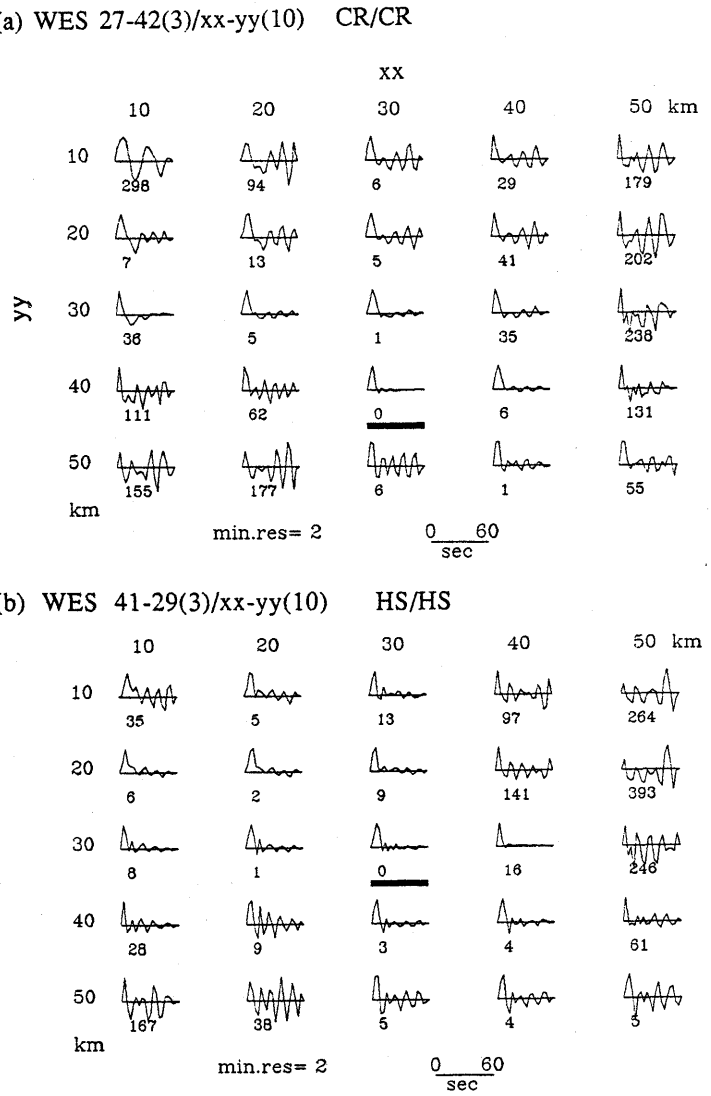

Fig. 2. (a) Source time functions from the long time deconvolution of the synthetic data; the data are synthesized for the rupture from 27 to 42 km point source depth with a grid interval of 3 km, which propagates with a velocity of 3 km/sec using solution CR. These are deconvolved by the GREEN's functions calculated using the same parameters but a grid interval of 10 km. This deconvolution is denoted by 27-42(3)/xx-yy(10) and CR/CR. The abscissa indicates the starting depth xx and the ordinate the final depth yy. The numeral below the source time function is the residual defined in the text. The value subtracting the minimum residual, whose value is shown in the bottom, is shown. The depth extent 30-40, indicated by the bar, gives the minimum residual and coincides with the model depth extent 27-42. (b) Long time deconvolution 41-29(3)/xx-yy(10) and HS/HS. Simple source time functions appeared at the point sources from 20 to 40 km depth.

depend much on the choice of the length allowed for the source time function unless we take a length comparable to the data, as will be discussed later.

Fig. 2a shows that the maximum source duration is less than 20 sec for all point sources. Fig. 3 shows the deconvolved source time functions for CR/CR and 27-42(3)/xx-yy(10) (the same as Fig. 2a) but the maximum source time function length is limited to be 24 sec; i.e., the number of variables m_i is seven. In this short time deconvolution, we do not need to use damping in the least squares solution because instability in the inversion does not occur. We obtain a minimum residual at 30-40 which agrees well with the depth extent (27-42) of the synthetics. The residuals at other depth ranges are larger by more than 2% than the minimum. We can now select the optimal solution as the one which gives the minimum residual. However, since parameters for the crustal structure, mechanism solution and rupture velocity used for the GREEN's functions may not necessarily be true ones, we next examine these effects using different parameters from those used in the synthetics.

3.2 Rupture velocity

The rupture velocity of the synthetics was varied from 1.5 km/sec to 4.5 km/sec in steps of 0.5 km/sec for CR/CR and 27-42(3)/xx-yy(10). These were deconvolved using a rupture velocity of 3 km/sec. The minimum residual was obtained at 30-40 with a variance reduction similar to that

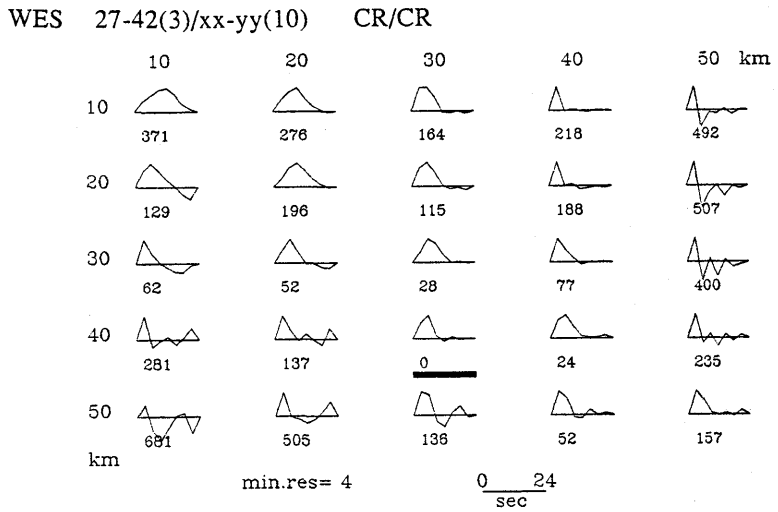

Fig. 3. Short time deconvolution 27-42(3)/xx-yy(10) and CR/CR. The minimum residual appeared at 30-40, which is expected from the model depth extent.

in Fig. 3 except for the velocity of 1.5 km/sec. For 1.5 km/sec, 20–20 and 30–50 give a minimum. If we assume an instantaneous vertical rupture for the synthetics, the minimum was obtained at 30–30. These results show that unless the rupture is very slow or too fast, the depth extent is retrieved correctly.

3.3 Crustal structure

We found that the deconvolution is most sensitive to the water layer-crustal structure. The synthetics generated using structure C1 shown in Table 2 (4.5 km thick water layer+4 layered crust/mantle) is deconvolved by the GREEN's functions calculated for difierent water layer thicknesses of 4.0 and 5.0 km; these are denoted by w4.5/w5.0, respectively (Figs. 4a and b). For w4.5/w4.0, the minimum residual is obtained at 40–50, deeper than the model depth extent (27–42), and the source time function at this depth extent is more complex than before (Fig. 4a). In contrast, for w4.5/w5.0, the minimum residual is 20–30, which is shallower than the model depth extent (Fig. 4b). These imply that the depth phases are advanced/delayed by a thinner/thicker water layer and are compensated by a deeper/shallower source depth. In both cases, the minimum residual and the residuals surrounding the minimum become larger than those in Fig. 3, i.e., the case of using the correct water depth.

Figs. 5a and b show examples of the long and short time deconvolutions, respectively, when we use a simpler crustal model in the kernel (C2: 4.5 km thick water layer+half space, Table 2), the same one as used in CHRISTENSEN and RUFF (1985). In the long time deconvolution, simple source time functions are obtained for the 20 and 30 km deep point sources, which are 10 km shallower than the model depth extent (Fig. 5a). If we use structure C2 in the deconvolution and the simplicity criterion to find the depth extent, we may obtain an incorrect rupture extent. In the short time deconvolution, the minimum residual was obtained at 30–40, but 40–50 also gives a similar residual. Those residuals become larger than the minimum in Fig. 3. Also the source time functions are skewed.

These experiments indicate that it is very important to use the correct water depth and crustal structure for the deconvolution. As for the crustal structure, when the epicenter is located in a normal ocean basin, we can use a typical oceanic crustal structure, such as C1 listed in Table 2. The water depth is more problematic because there is an error in epicentral location listed in seismological bulletins, usually amounting to a few tens of km. This may cause a large error in estimation of the water depth above the epicenter from a bathymetric chart. Therefore, in application

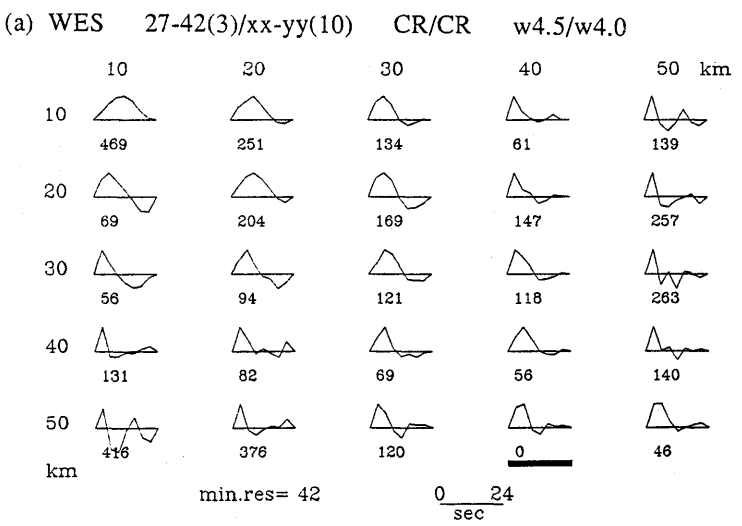

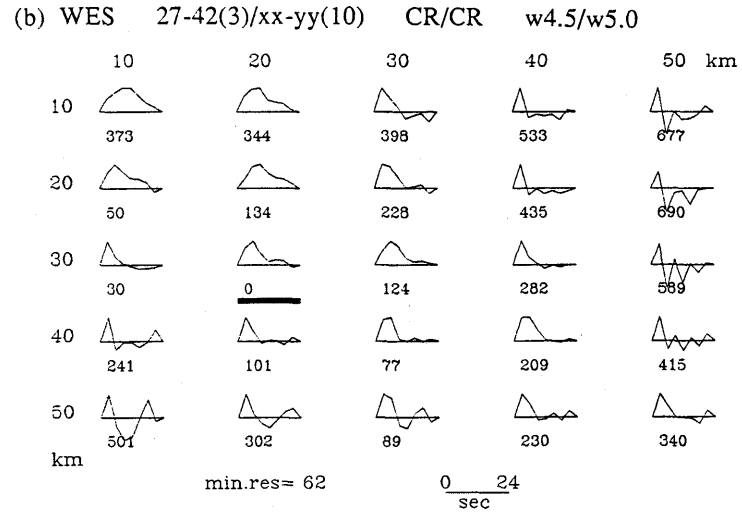

Fig. 4. (a) Short time deconvolution. The synthetic data using crustal structure C1 (Table 2) with a water layer thickness of 4.5 km are deconvolved with the same structure but water layer thickness of 4.0 km. The minimum residual location shifted to a deeper extent (40-50) than the model depth extent. (b) Short time deconvolution. The synthetic data using crustal structure C1 with a water layer thickness of 4.5 km are deconvolved with the same structure but water layer thickness of 5.0 km. The minimum residual location shifted to a shallower depth extent (20-30) than the model depth extent.

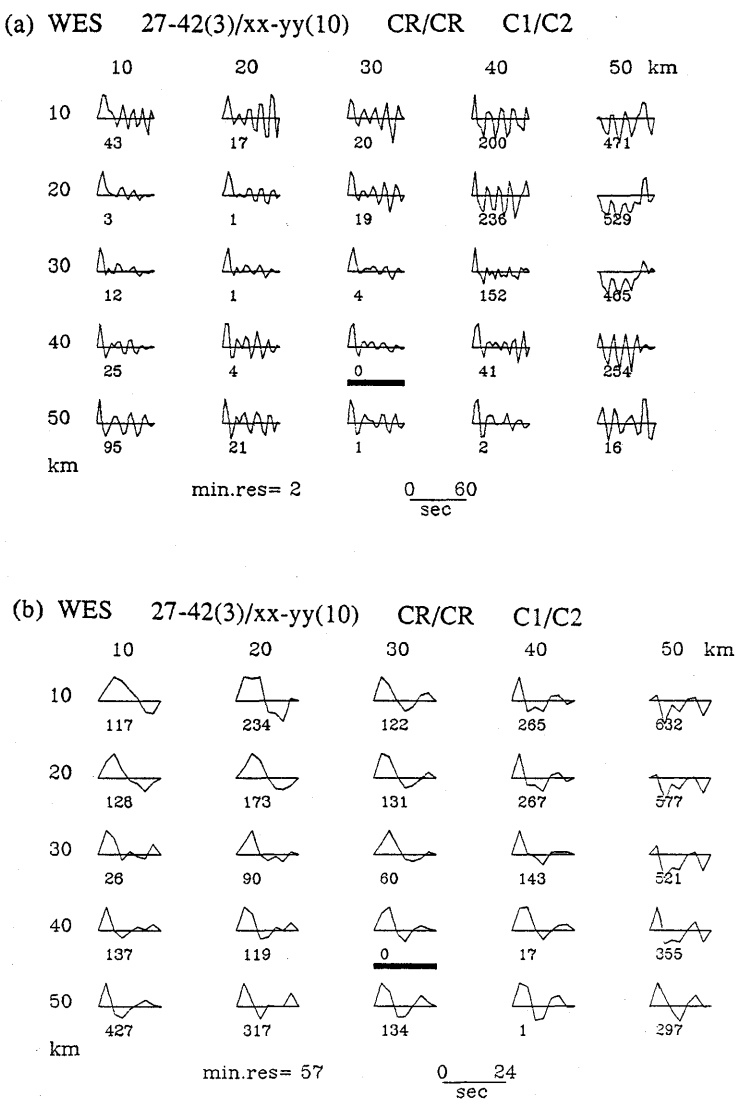

Fig. 5. (a) Long time deconvolution. The synthetic data using crustal structure C1 are deconvolved by structure C2 (Table 2). Simple source time functions appeared from 20 to 30 km point source depth. (b) Short time deconvolution. The synthetic data using crustal structure C1 are deconvolved by structure C2. The source time function is skewed at 30-40 and the minimum residual increased compared to Fig. 3.

to a real earthquake, we have to see how the residual and source time function vary along with the assumed water depth used in the kernel. We will show an example in the application of this method to the Chile earthquake.

3.4 Mechanism solution

We finally examined the effect of the mechanism solution on the deconvolution. Fig. 6 shows the deconvolution results for CR/HS and 27-42(3)/xx-yy(10); that is, the synthetics using solution CR are deconvolved by solution HS. In this case, the minimum residual is obtained at 40-40, shifted to the deeper end of the model depth extent. We found that this kind of shift to a nearby depth extent often occurs when we change one of the source parameters (strike, dip and slip angles) by 10 degrees. We can see that the deconvolution is sensitive to uncertainty in the mechanism solution. Since uncertainty amounting to 10 degrees is usual, we also have to take into account this effect. In the analysis of the 1981 Chile earthquake, we will use both solutions CR and HS, and examine the effect of the different solutions.

4. Analysis of the Chile earthquake of October 16, 1981

4.1 Deconvolution

The October 1981 Chile earthquake (M_S=7.2) occurred in the outer-

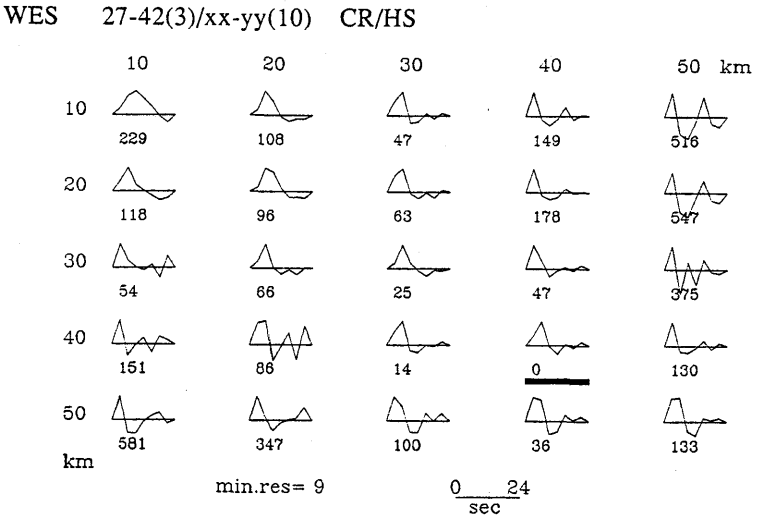

Fig. 6. Short time deconvolution. The synthetic data using solution CR are deconvolved by solution HS. The minimum residual location shifted deeper, to 40-40, than the model depth extent.

rise area off the Chilean coast (Fig. 1a). We use WWSSN long-period P-waves at the five stations shown in Fig. 1b as data. These records are digitized and sampled at a rate of 1 Hz for the first 60 sec from the onset of P. Fig. 7a shows the long time deconvolution at WES, using mechanism CR and crustal structure C1. The 4.5 km water depth is used for this case; this is the observed water depth above the epicenter in the bathymetric chart (MAMMERICKX *et al.*, 1975). Below we will see that this is

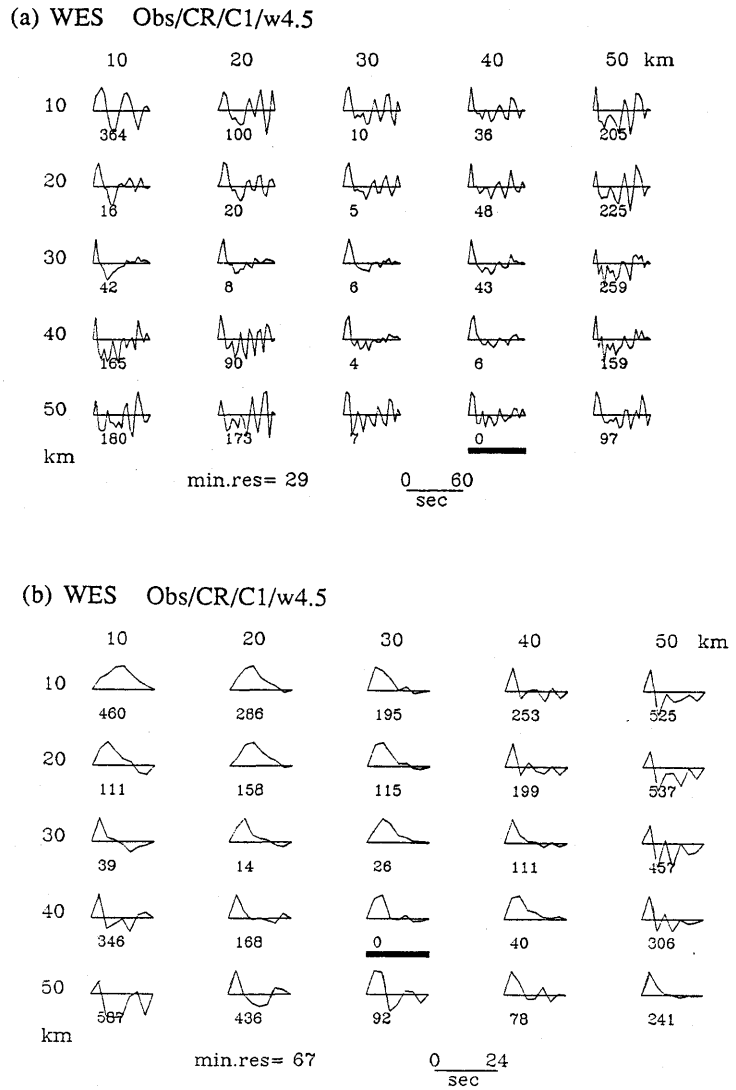

Fig. 7. (a) and (b) Long and short time deconvolutions Obs/CR/C1/w4.5 at WES.

the optimal estimate for the water depth. This deconvolution is denoted by Obs/CR/C1/w4.5. Simple source time functions are obtained for the depth ranges from 30 to 40 km (Fig. 7a). From the source time functions assuming point sources, we can find that the maximum source duration is less than 15 sec. The long time deconvolution using solution HS is shown in the appendix (Fig. A1). Fig. 7b shows the short time deconvolution using 24 sec for the maximum length allowed for the source time function; other parameters are the same. We obtain the minimum residual 67 (6.7%) at 30-40; however, 20-30 and 30-30 also give small residuals (81 and 93). (The short time deconvolution using solution HS at WES is shown in Fig. 12).

We examine here the water depth above the epicenter. Figs. 8a and b show deconvolutions Obs/w4.0 and Obs/w5.0 at WES, respectively. As the water depth increases, the minimum is obtained at the shallower depth, which is the observed behavior in the synthetic data experiment (Figs. 3 and 4). The minimum residual becomes larger (179) for Obs/w5.0 than for Obs/w4.5 (67). In the case of Obs/w4.0, the minimum residual did not change much (63), but the residuals around the minimum increased. Also note that the source time function becomes more complex at the minimum. These features are also seen when we use solution HS. Thus we take 4.5 km as the optimal estimate for the water depth above the epicenter.

The short time deconvolution results for other stations using CR are shown in Fig. A2, and those using HS in Fig. A3, in the appendix. For both mechanism solutions, the depth extents of 30-40 and 40-30 or point sources around this depth range are obtained except for RAR. For RAR, a shallower depth extent 20-10 is obtained for both solutions. However, for this station, note that there is a local minimum in residual at 30 km point source. Fig. 9a summarizes the depth extents obtained using 10 km grid spacing.

In the above short time deconvolutions, we can see that there is not much difference in residual between 30 and 40 km point sources (Figs. 7b, A2, 12a and A3). This suggests that the centroid depth is probably located between these depths. Also there is no preference for a finite rupture. This indicates that the depth extent is not so large as it covers two grid points completely. Because it seems that a 10 km grid spacing is too coarse to find the depth extent, we conducted deconvolution using 5 km grid spacing. Ruptures containing one or two grid points around 30-40 km depth are obtained as optimal solutions for both mechanism solutions as shown in Fig. 9b; for example 35-35 for CR and 35-30 for HS are obtained at

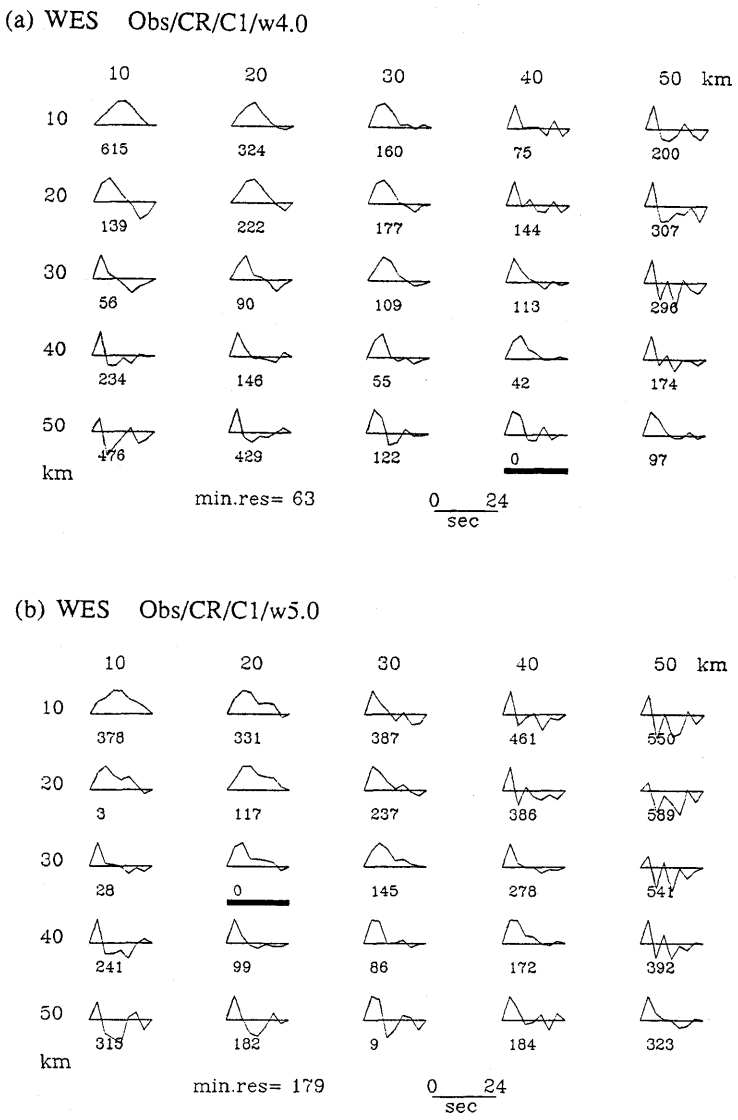

Fig. 8. (a) and (b) Short time deconvolutions Obs/CR/C1/w4.0 and Obs/CR/C1/w5.0, respectively. The minimum residual location shifted to deeper and shallower depth extents than 30-40 (Obs/CR/C1/w4.5) in Fig. 7(b). The residuals around the minimum are increased in both cases.

RAR. However, the variance reduction of the optimal solution from other rupture modes is very small in the deconvolution using 5 km grid spacing. Fig. 10 shows an example of the deconvolution at LON. The variance reduction is less than a few percent for many rupture modes. The GREEN's function would not change much within the depth of 5 km

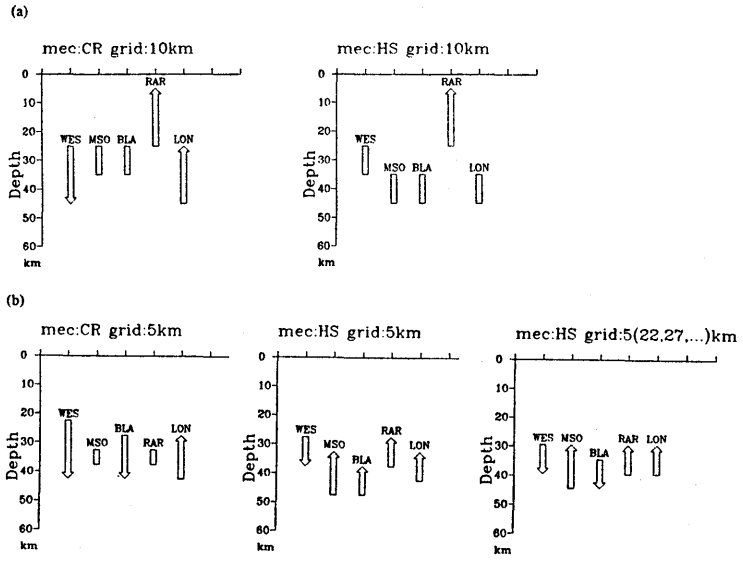

Fig. 9. Summary of the depth extents obtained by short time deconvolution of the observed data. (a) Results of Obs/xx-yy(10)/CR and Obs/xx-yy(10)/HS. The point source is represented by a bar with a length of 10 km at its depth. (b) The results of Obs/xx-yy(5)/CR and Obs/xx-yy(5)/HS. The point source is represented by a bar with a length of 5 km at its depth. For the latter, the results when the grid points are shifted by 2 km are also shown.

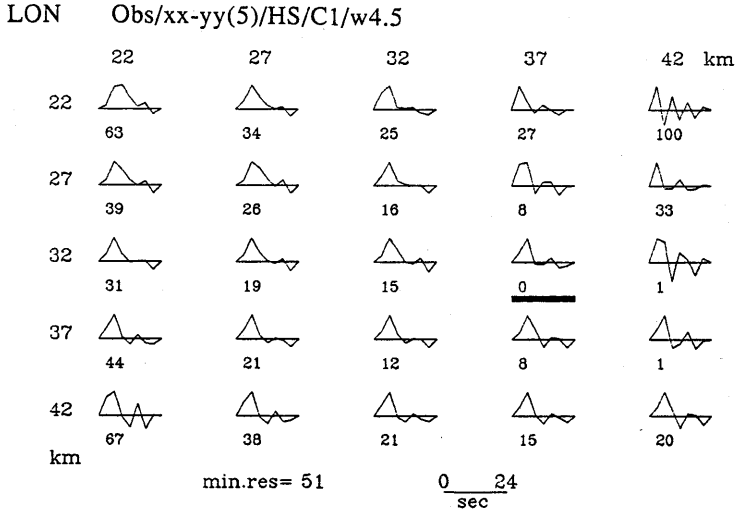

Fig. 10. Short time deconvolution Obs/xx-yy(5)/HS/C1/w4.5 at LON. There are many depth extents which give a small residual contrast from the minimum.

or so and a difference of 5 km cannot be well resolved from the observed data, if we allow the number of free parameters in the source time function to be as large as seven.

4.2 Synthetic data experiment

Although the above deconvolutions show that the centroid depth of the Chile earthquake is located around 35 km and that the depth extent is not much larger than 10 km, we failed to elucidate the finite depth extent by the present method. Below, in order to supplement the results above, we conduct several synthetic data/deconvolution experiments.

First, we examine which of the mechanism solutions, CR or HS, is preferred. Synthetic data are generated using either HS or CR assuming a point source located at 35 km depth and an isosceles triangular source time function (5, 0, 5). This width is consistent with the results from the observed data obtained at 30–40 km point source depth. These data are then deconvolved by the kernels using either CR or HS. Figs. 11a and b show the long time deconvolutions, HS/CR and CR/CR, respectively. The deconvolution of HS/CR produced very similar source time functions to those deconvolved from the observed data (Obs/CR) (Fig. 7a). In contrast, CR/CR results are very different from those of Obs/CR. The deconvolved moment rates m_i in Figs. 11a and b show the correlation coefficients with those in Fig. 7a, averaged over all the depth ranges, of 0.969 and 0.881, respectively. These phenomena are also observed when we did deconvolutions HS/HS and CR/HS and compared them with Obs/HS. HS/HS is very similar to Obs/HS but CR/HS is not. From these experiments, we may say that HS is closer to the mechanism solution than CR.

Next, we examine the centroid depth and depth extent. We compare the deconvolution results of the synthetics generated from various controid depths and depth extents and compare them with the deconvolution results of the observed data. In the synthetics, we use solution HS for the reason described above. Three centroid depths at 35, 30 and 25 km and the vertical depth extents of 3, 9, 15 and 21 km (over 1, 3, 5, and 7 grid points with a 3 km interval, respectively) are tested. The source time function assumed in the synthetics is of an isosceles triangular shape. The isosceles triangular shape assumption is simple but the following results did not change even if we use other shapes. The source time function width is determined so that the total source duration becomes 10, 11 and 12 sec for 35, 30 and 25 km centroid depth, respectively, which are consistent with the results from the observed data. We did not use station RAR, since the data are of poor quality.

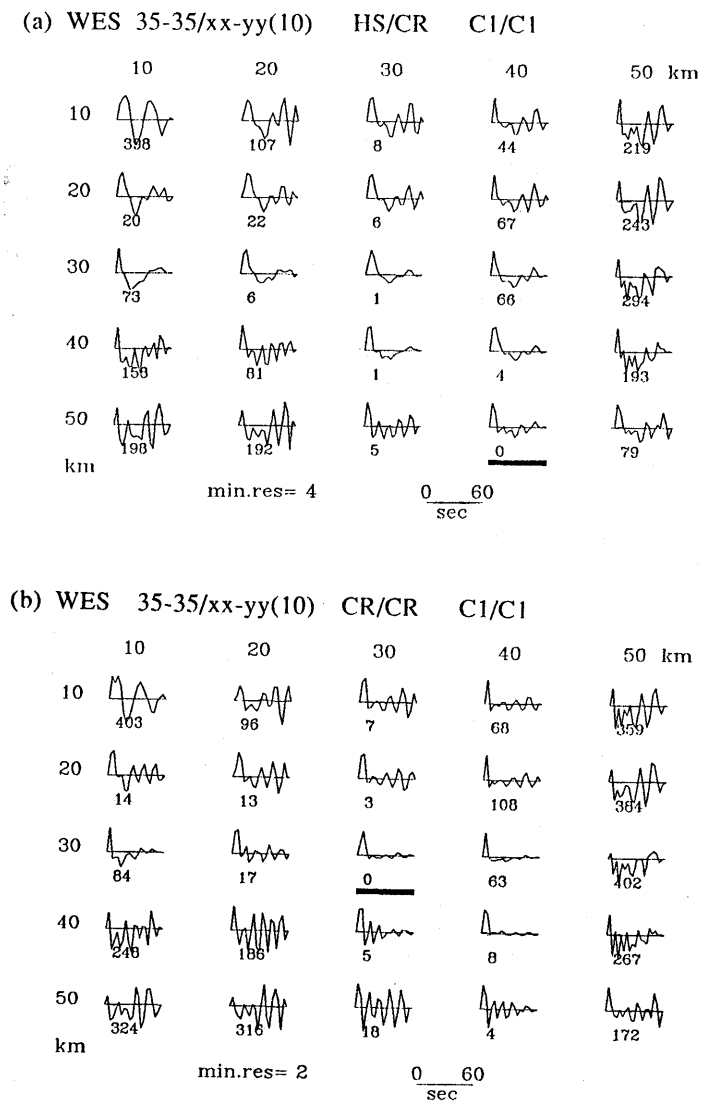

Fig. 11. (a) and (b) Long time deconvolutions 35-35/xx-yy(10) and HS/CR and CR/CR, respectively. The former shows a striking similarity in the shape of the source time functions to those obtained from Obs/CR (Fig. 7a), but the latter did not show such a similarity.

Fig. 12a shows the short time deconvolution Obs/HS/C1/w4.5 from the observed data at WES (see Fig. A3 for other stations). The essential feature of the residual pattern common to all stations is that the smallest residuals appear at the 30 km and 40 km point sources. The residuals at 30-40 or 40-30 are slightly larger than them; for WES and BLA, the

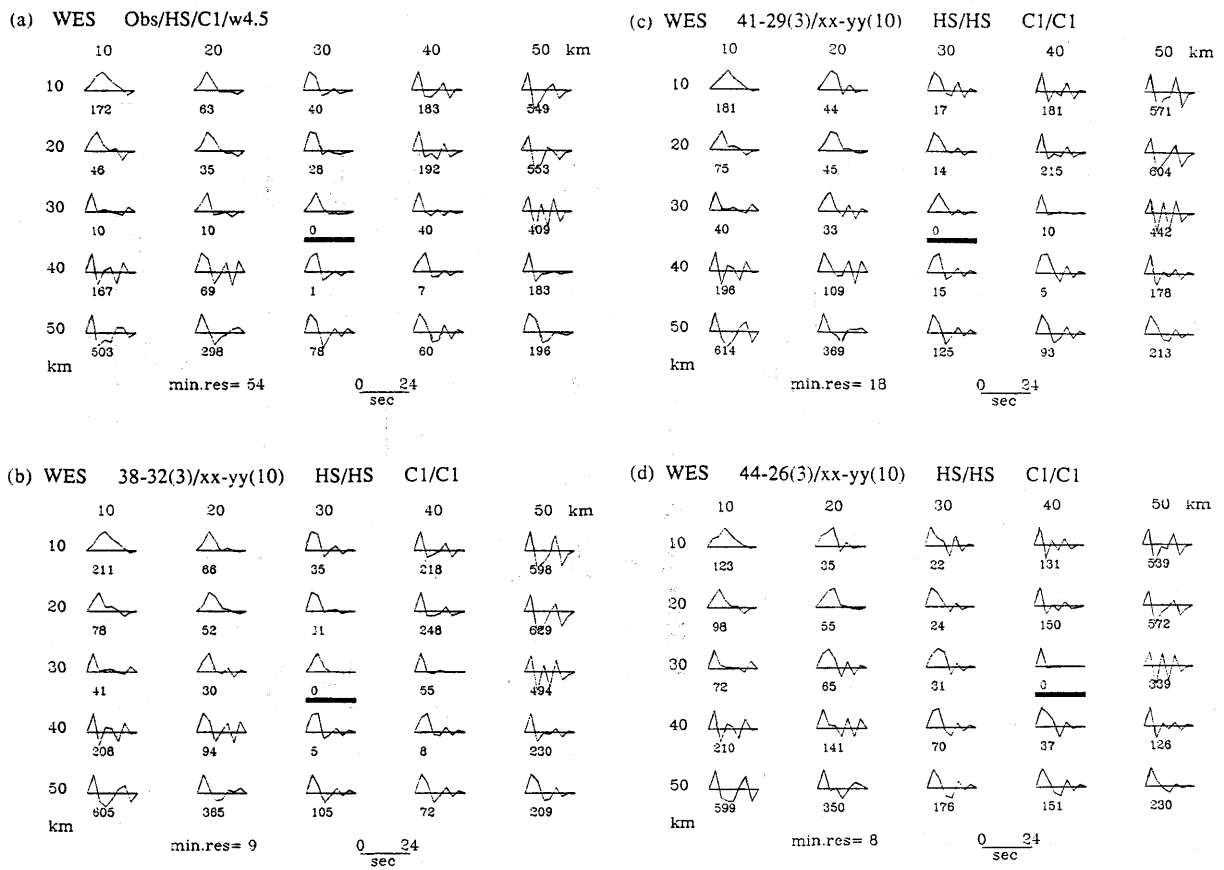

Fig. 12. (a) Obs/HS/C1/w4.5 at WES. (b), (c), (d) 38-32(3), 41-29(3) and 44-26(3) are deconvolved by a 10 km grid spacing, using solution HS and structure C1. (b) and (c) show the similarity in residuals around 30-40 km depth to (a) and those in Fig. A3, but (d) produces a strong minimum residual at 40-30.

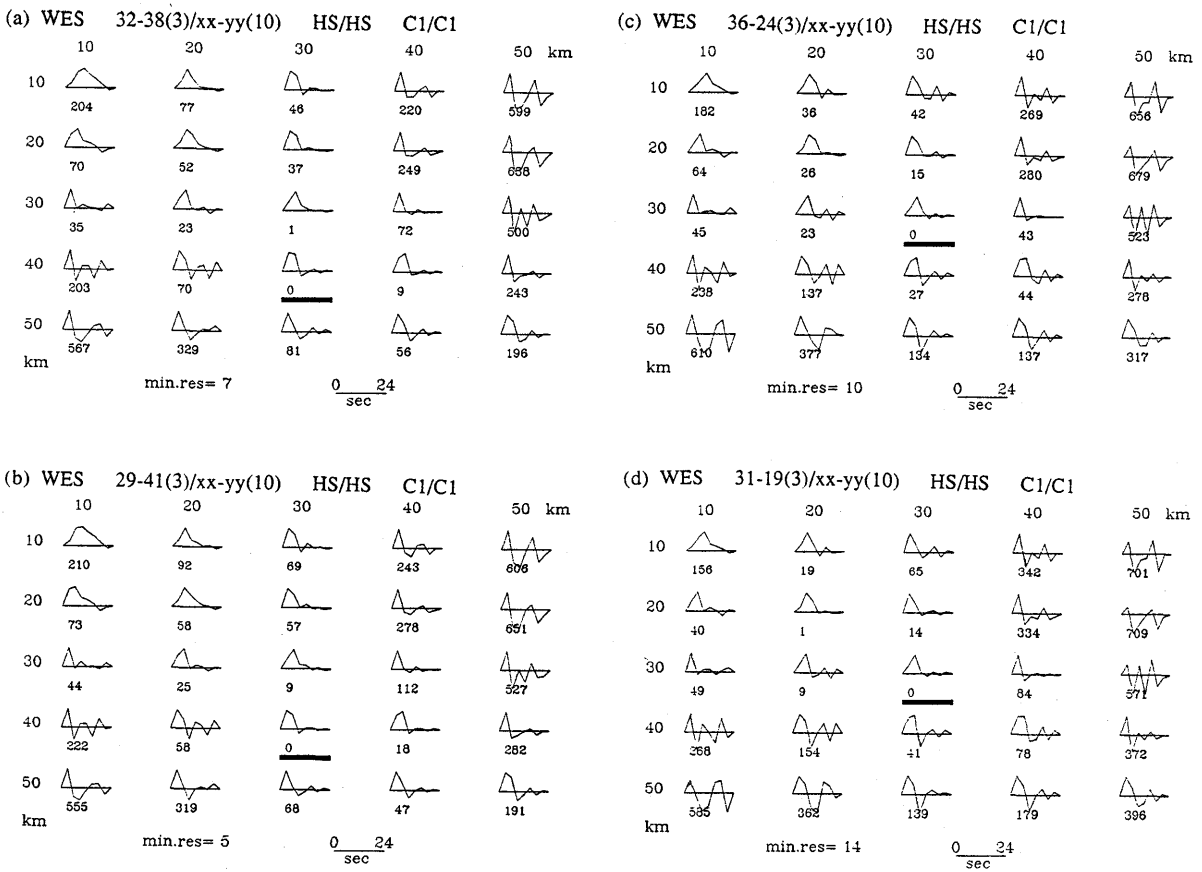

Fig. 13. (a), (b), (c) and (d) 32-38(3), 29-41(3), 36-24(3) and 31-19(3) are deconvolved by a 10 km grid spacing and solution HS and structure C1. (a) and (b) produce larger residual at 40-30 than that from the observed data (Fig. 12 and Fig. A3). (c) and (d) produce small residuals at shallower depths than those from observed data.

residual at 40-30 is larger by a few percent than that at 30-40, but they are almost the same for MOS and LON. We try to seek a centroid depth and depth extent which explain these features.

Figs. 12b, c and d show the deconvolutions at WES using synthetics for which centroid is located at 35 km and the rupture propagates upward. In Fig. 12b, where the source has 9 km depth extent (38-32(3)), we can see the features mentioned above; the residuals at 30-30, 40-40 and 30-40 are very small. Moreover, the shapes of the deconvolved source time functions are strikingly similar to those from the observed data (Fig. 12a). In the results of deconvolution of 41-29(3) (Fig. 12c), whose synthetics represent a 15 km depth extent, we can still see the above features. However, the deconvolution of 44-26(3), i.e. the 21 km depth extent, shows a strong minimum at 40-30, with a few to several % contrast to 30-30, 40-40 and 30-40 (Fig. 12d).

Figs. 13a and b show the deconvolutions of the synthetics representing the downward ruptures with extents of 9 and 15 km centered at 35 km, respectively. In these cases the residual at 40-30 becomes larger (72 and 112) than that deconvolved from the observed data.

Figs. 13c and d show the deconvolutions of the synthetics representing the upward rupture centered at 30 and 25 km, respectively, with a 15 km depth extent. In these cases, the smallest residuals appear at shallower depths than the deconvolutions of the synthetics centered at 35 km. Note that the residual at 40-40 is larger than that of the deconvolution of the observed data. From the comparison above, we take the upward rupture with a 9-15 km depth extent centered at 35 km as our preferred solution.

Finally we show the fit of the synthetic data to the observed data in Fig. 14. The synthetic data are from the optimal solution of the short time deconvolution of Obs/HS/C1/w4.5. We also show the comparison between the observed data and the synthetics from the optimal solution of the deconvolution in which the GREEN's functions are calculated using 41-29(3) or 29-41(3) rupture and assuming a single isosceles triangle source time function. The width of the triangular source time function used is

Fig. 14. Comparison of the observed data with synthetics. The synthetics are from the solution which gives the minimum residual in the short time deconvolution. Left; Obs/xx-yy(10)/HS/C1. The unit triangle of the moment rate function is (3, 0, 3) and total number is seven. Middle; Obs/41-29(3). The unit triangle of the moment rate function is (2.3, 0, 2.3) and only one triangle is used in the deconvolution. Right; Obs/29-41(3). The unit triangle of the moment rate function is (3.7, 0, 3.7) and only one triangle is used in the deconvolution. The obtained seismic moments are shown in units of 10^{25} dyn·cm.

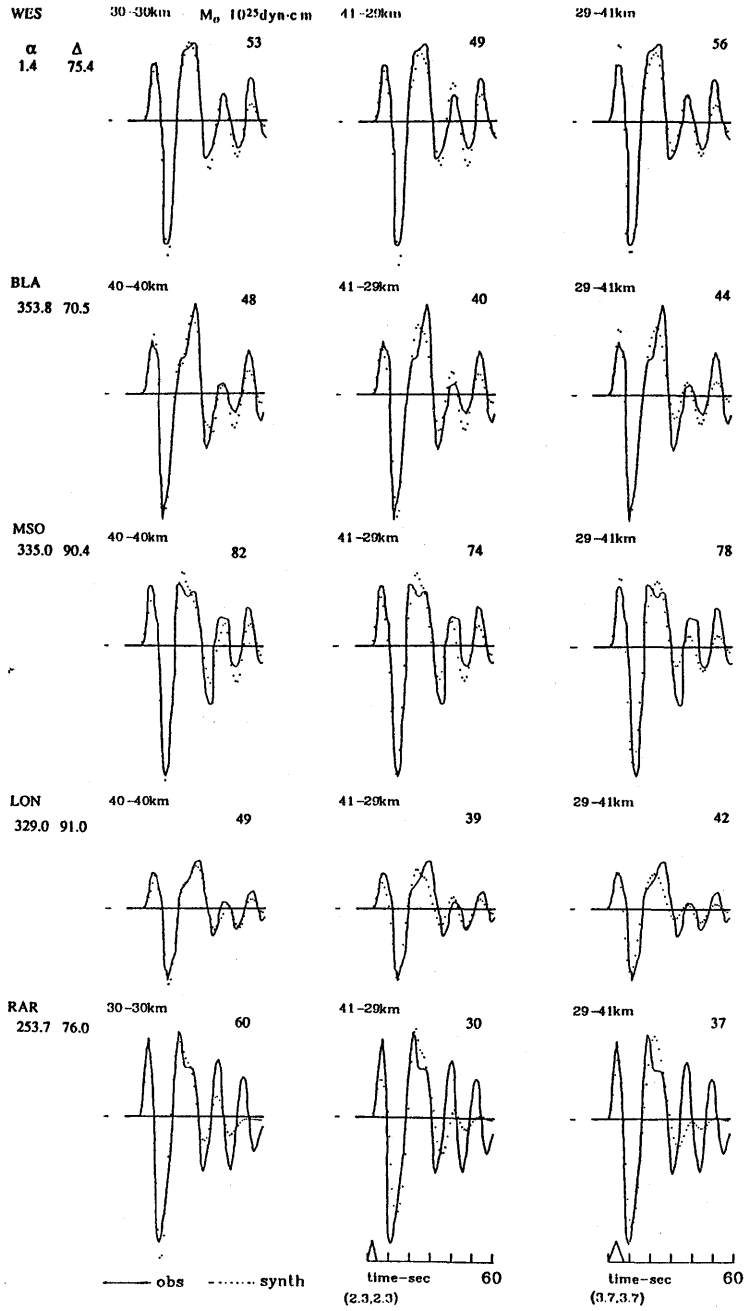

the same one used in the synthetic data experiments above.

The seismic moments (the sum of the positive moments m_i) are also shown. The average of the seismic moment for the optimal solution

using the 10 km grid spacing is 5.8×10^{26} dyne·cm. This coincides with the value obtained by HONDA and SENO (1989) (5.8–6.3×10^{26} dyne·cm) in which moment tensor inversion of both the body and surface wave data was conducted simultaneously.

Using the depth extent of 12 km (average of 9 and 15 km), the fault width is estimated to be 17 km assuming a dip of 45 degrees. The fault length is estimated to be 15 km as follows. The width of the source time function, which represents horizontal rupture, is 6 sec for this vertical extent. We estimate the horizontal rupture time to be 5 sec, subtracting 1 sec, needed to vertically rupture each 3 km segment, from the above 6 sec. This is multiplied by the 3 km rupture velocity. The average dislocation is 3.3 m using the seismic moment of 5.8×10^{26} dyne·cm assuming a rigidity μ of 7×10^{11} dyne/cm^2. The stress drop is calculated to be 350 bars assuming a circular fault which has the same fault area.

5. Discussion

5.1 Effect of water depth and crustal structure

CHRISTENSEN and RUFF (1985) obtained a shallower depth extent for this event using a simple crustal structure, i.e., water layer+half space (C2, Table 2). In C1/C2, we have shown that simple source time functions are obtained at the shallower depths than the depth extent used in the synthetics (Fig. 5a). This may be the cause of the difference between the present results (41–29 km) and those of CHRISTENSEN and RUFF (1985) (5–25 km). We here demonstrate this by deconvolving the observed data by C2. Fig. 15 shows the long time deconvolution Obs/CR/C2 at WES. Simple source time functions were obtained at shallower depths than Obs/CR/C1 (c.f., Fig. 7a). If we use the measure of simplicity used by CHRISTENSEN and RUFF (1985), we would obtain 10–30 km as the depth range of this event, which is similar to the results obtained by them (5–25 km). We have already shown that even if we use the correct crustal structure in the GREEN's functions, a simple source time function may be obtained at the shallower depth than the model depth extent (Fig. 2b). Therefore it may be dangerous to use the simplicity criterion for the purpose of finding the depth extent.

5.2 Choice of the maximum length of the source time function

We set the maximum length of the source time function as 24 sec in the short time deconvolution. We examined the effect of change in this length on the residual. We varied the length from 15 sec to 36 sec in 3 sec steps and deconvolved the observed data at WES. For 10 km grid

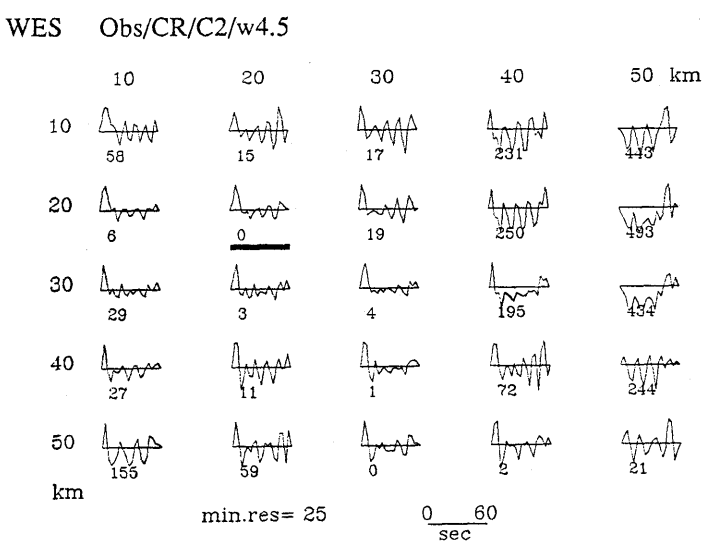

Fig. 15. Long time deconvolution Obs/CR/C2/w4.5 at WES. Simple source time functions appeared at 20-30 km point source depths.

spacing, the residual pattern did not change. The minimum residual was obtained at 30-40, 30-30 or 40-40 for Obs/HS and 30-40 for Obs/CR. Since the residuals are almost the same among 30-40, 30-30 and 40-40 for Obs/HS (Fig. 12 and Fig. A3), the minimum residual location may be unstable among these depth extents. In contrast, for Obs/CR, 30-40 is the minimum with a larger variance reduction from other depth extents (Fig. 7b), resulting in stability of the minimum location.

5.3 Reliability

We discuss some crucial points on the reliability of the solution. The minimum residuals of the short time deconvolution Obs/HS (Fig. 12a and A3) amount to 5-6% except for RAR (13.8%) and MSO (8.7%). The variance reduction of the minimum residual compared to the surrounding rupture modes is less than a few percent. The variance reduction over 1/1.67 is required to be significant at the 95% confidence level in the F-test when the number of degrees of freedom is 53 (60 data minus 7 free parameters in m_i); thus a reduction of 3-4% in residual is required at the residual level of 5-6% to be significant in the F-test. Therefore we cannot distinguish the superiority among 30-30, 40-40, 30-40 and 40-30 statistically in the short time deconvolution. This is not surprising because the fault is likely to be located around these depths. There are, however, some other depth extents which give a small residual; e. g., 10-30 at WES (1% difference from the minimum) and 30-10 at LON (1.8%

difference from the minimum). However, these small residuals are not common to all stations, and probably have been produced by random noise in the data.

In the synthetic data/deconvolution experiments, we have seen that ruptures with a vertical extent less than 21 km centered at 35 km depth produced a very similar pattern in the source time functions and residuals from those deconvolved from the real data. Although we took an upward rupture of 12($\pm$3) km vertical extent centered at 35 km depth as the optimal solution in this study, it is not straightforward to assess the reliability of the solution. Looking at the variation in residuals in the deconvolution of the observed data among different stations, we can guess that the random noise in the data would amount to at least a few percent of the data variance. Even if the random errors are contained in the data, the overall pattern of the residuals would not change much from those deconvolved from the error-free data. The remaining residual at the minimum would have resulted from the fact that the GREEN's functions calculated in this paper are different from the true ones. The use of the true GREEN's fuuctions, if possible, would change the deconvolution results to some extent. Although we tried to use realistic parameters in the calculation of the GREEN's functions, it is not possible to remove the difference completely. The most serious difference may come from the fact that the sea floor has a dip, which may modify the GREEN's function (WIENS, 1987; OKAMOTO and MIYATAKE, 1989). Since the effect of the dip of the sea floor is remarkable in the later phases, the discrepancy between the observed and synthesized seismograms shown in Fig. 14, which shows a larger difference in the later phases, might have originated from this effect.

Another source producing the difference from the true GREEN's functions would be our simplified assumption for the rupture process. We assumed a uniform mechanism solution for any grid points. We have to be careful when we apply the method of the present study to large subduction zone earthquakes. However, for the case of the Chile earthquake, the studies of the source of this event using both body and surface waves indicate that a single double couple represents the source very well (HONDA aud SENO, 1989; HONDA *et al.*, 1990) and the size of the event is small enough to be represented by a point source; thus this effect would not be serious. Although it is not possible to evaluate at present how much the location of the minimum residual would change from those in Fig. 12a and Fig. A3 when we use the true GREEN's fuuctions, the striking similarity between the deconvolution of the synthetic data whose centroid is located at 35 km and that of the observed

data (Figs. 12a, b and c) suggests that our GREEN's functions are not far from the true ones.

5.4 Tectonic implications

The obtained depth extent corresponds to 25–35 km depth below the sea floor. The lower limit of the mechanical thickness of the lithosphere, within which earthquakes can occur, is defined by the 750°C isotherm of the plate model (WIENS and STEIN, 1984; SENO *et al.*, 1990). The mechanical thickness thus defined is about 35 km at 40 Ma, which is the age of the Nazca plate where the epicenter is located (HALBOUTY *et al.*, 1981). Thus the 1981 Chile earthquake ruptured only the lower portion of the mechanical lithosphere.

The stress disturbance due to recurrence of large interplate earthquakes at the thrust zone is on the order of the stress drop of those earthquakes, that is, less than 100 bars (KANAMORI aud ANDERSON, 1975). On the other hand, the local tectoinc stresses due to the combination of the ridge push, slab pull and thrust zone interaction are on the order of 1 kbar at most (PARSONS and RICHTER, 1980; DAVIES, 1983; FROIDEVAUX *et al.*, 1988). The results of this study indicate that the bending stress is likely to be larger by one order of magnitude than these tectonic stresses in this region, because the neutral plane of the bending stress did not show any significant shift at the time of the Chile earthquake. Rheological implications for oceanic plates will be treated in a separate paper, including the results in other regions (SENO *et al.*, 1990).

6. Conclusions

We present a method to retrieve a vertical rupture extent of a large shallow earthquake of which the rupture mode is assumed to be simple. In this method, the observed seismogram is deconvolved by the GREEN's functions calculated for various finite depth extents with constant upward or downward rupture propagation. We tested this method by synthetic data experiments and found that the assumed crustal structure, especially, the water layer thickness, significantly affects the deconvolution results. We also found that the simplicity criterion, used by CHRISTENSEN and RUFF (1985), is not useful for retrieving the correct depth extent.

We applied the above method to the 1981 Chile earthquake (M_S=7.2), and obtained 30 or 40 km deep point sources as optimal solutions. This earthquake is not large enough for this method to be applied effectively. We supplemented the obtained results by conducting synthetic data/decon-

volution experiments. The synthetics generated for a depth extent of 12 km (±3 km) centered at 35 km depth give the deconvolution results most similar to those from the observed data. We also found that the mechanism solution of HONDA and SENO (1989) is preferred to that of CHRISTENSEN and RUFF (1985). The GREEN's functions used in this study still do not explain a few percent of the variance of the observed waveform. Future studies, including the effect of the dipping sea floor in the GREEN's functions, are necessary to improve the results obtained in this study.

The obtained depth extent from 40 to 30 km below the sea surface shows that the neutral plane of the bending stress of the Nazca plate was not shifted at the time of this earthquake. This would provide an important piece of information on the strength of the lithosphere (e. g., GOETZ and EVANS, 1979; WIENS and STEIN, 1985), and on the ways of interaction between large interplate earthquakes and intraplate slab and outer-rise events (CHRISTENSEN and RUFF, 1988; DMOWSKA *et al.*, 1988; LAY *et al.*, 1989; ASTIZ *et al.*, 1989).

Acknowledgements

We acknowledge the criticisms of Bob Geller and one anonymous reviewer, and discussions with Hitoshi KAWAKATSU.

Appendix

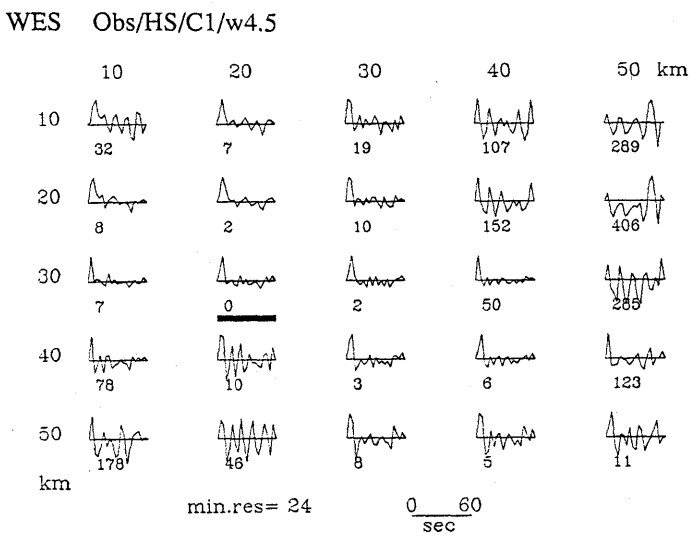

Fig. A1. Long time deconvolution Obs/HS/C1/w4.5; this is already reported in HONDA *et al.* (1990).

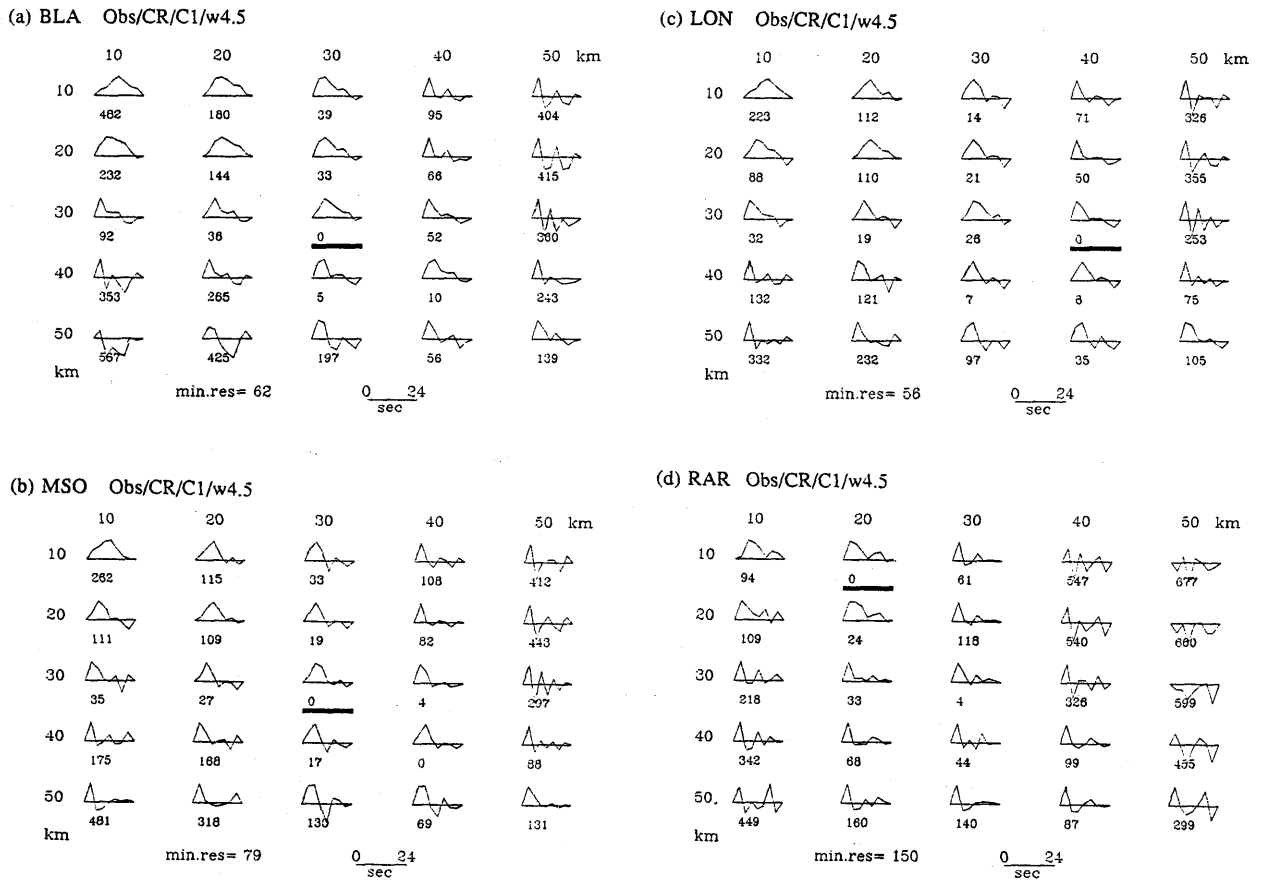

Fig. A2. Short time deconvolutions Obs/CR/C1/w4.5 at stations other than WES.

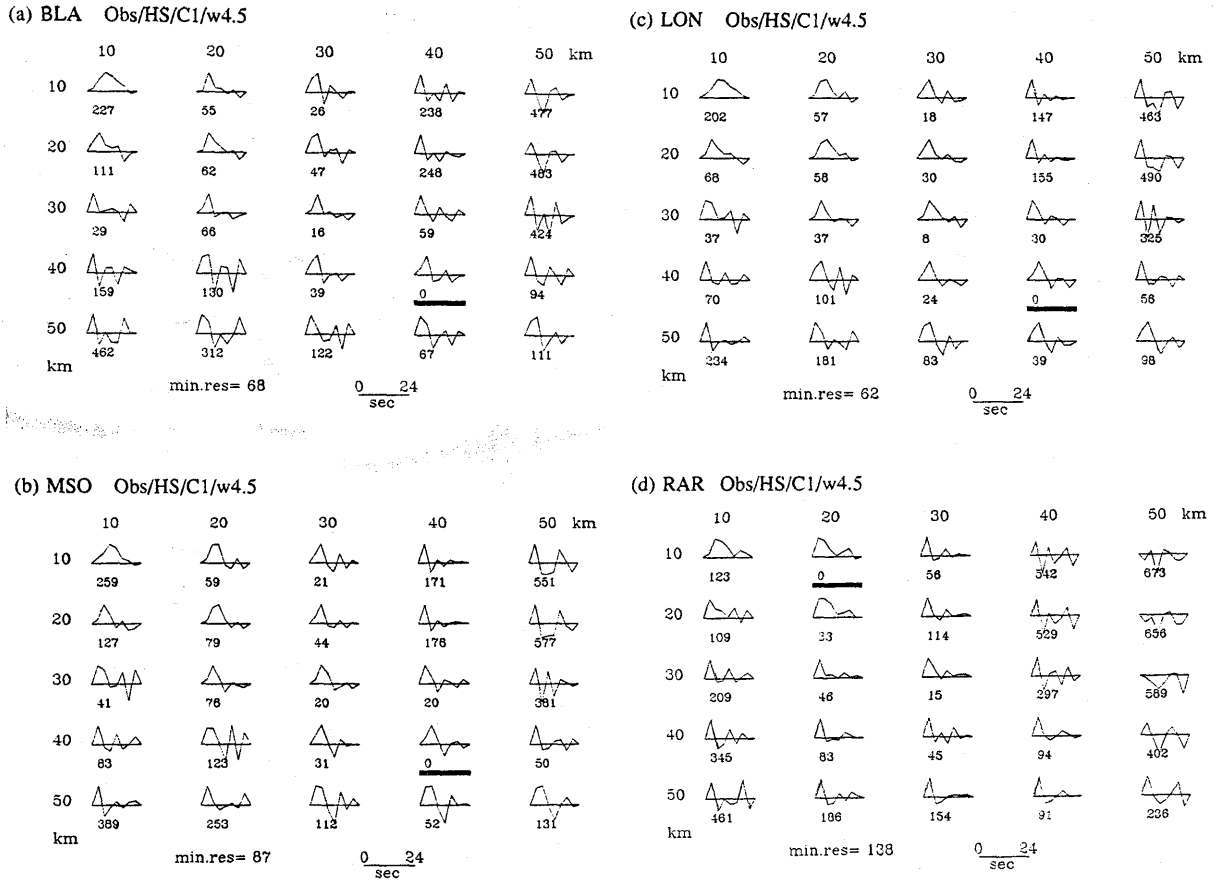

Fig. A3. Short time deconvolutions Obs/HS/C1/w4.5 at stations other than WES. The preliminary results of these deconvolution are already reported in HONDA *et al.* (1990).

References

ASTIZ, L., T. LAY and H. KANAMORI, 1988, Large intermediate-depth earthquakes and the subduction process, *Phys. Earth Planet. Inter.*, 53, 80–166.

CARPENTER, E. W., 1966, Absorption of elastic waves-An operator for constant Q mechanism, *Res. O-43/66, At. Weapons Res. Estab., Her Majesty's Stationery Office, London.*, 16pp..

CHRISTENSEN, D. H. and L. J. RUFF, 1985, Analysis of the trade-off between hypocentral depth and source time function, *Bnll. Seism. Soc. Am.*, **75**, 1637–1656.

CHRISTENSEN, D. H. and L. J. RUFF, 1988, Seismic coupling and outer-rise earthquakes, *J. Geophys. Res.*, **93**, 13421–13444.

DAVIES, G. F., 1983, Subduction zone stresses: constraints from mechanics and from topographic and geoid anomalies, *Tectonophysics*, **99**, 85–98.

DMOWSKA, R. J., R. RICE, L. C. LOVINSON and D. JOSELL, 1988, Stress transfer and seismic phenomena in coupled subduction zones during earthquake cycle, *J. Geophys. Res.*, **93**, 7869–7884.

FORSYTH, D. W., 1982, Determination of focal depths of earthquakes associated with the bending of oceanic plates at trenches, *Phys. Earth Planet. Inter.*, 28, 141–160.

FROIDEVAUX, C., S. UYEDA and M. UYESHIMA, 1988, Island arc tectonics, *Tectonophysics*, **148**, 1–9.

GOETZE, C. and B. EVANS, 1979, Stress and temperature in the bending lithosphere as constrained by experimental rock mechanics, *Geophys. J. R. astr. Soc.*, **59**, 463–478.

HALBOUTY, M. T., J. A. REINEMUND and M. J. TERMAN, 1981, Plate-tectonic map of the circum-Pacific region, *Circum-Pacific Council for Energy and Mineral Resources.*

HERRIN, E., 1968, Introduction to "1968 seismological tables for p phases", *Bull. Seism. Soc. Am.*, 58, 1193–1225.

HONDA, S. and T. SENO, 1989, Seismic moment tensors and source depths determined by the simultaneous inversion of body and surface waves, *Phys. Earth Planet. Inter.*, **57**, 311–329.

HONDA, S., H. KAWAKATSU and T. SENO, 1990, Centroid depth of the October 1981 off Chile outer-rise earthquake (M_S=7.2) determined by a comparison of several waveform inversion methods, *Bull. Seism. Soc. Am.*, in press.

KANAMORI, H. and G. S. STEWART, 1976, Mode of the strain release along the Gibbs fracture zone, mid-Atlantic ridge, *Phys. Earth Planet. Inter.*, **11**, 312–332.

KANAMORI, H. and D. L. ANDERSON, 1975, Theoretical basis of some empirical relations in seismology, *Bull. Seism. Soc. Am.*, **65**, 1073–1095.

KROEGER, G. C. and R. J. GELLER, 1983, An efficient method for computing synthetic reflection seismograms for plane layered models, *EOS, Trans. Amer. Geophys. Union*, **64**, 772.

LAY, T., D. H. CHRISTENSEN, L. ASTIZ and H. KANAMORI, 1989, Temporal variation of large intraplate earthquakes in coupled subduction zones, *Phys. Earth Planet. Inter.*, **54**, 258–312.

LISTER, C. R. B., 1975, Gravitational drive on oceanic plates caused by thermal contraction, *Nature*, **257**, 663–665.

MAMMERICKX, J., S. M. SMITH, I. L. TAYLOR and T. E. CHASE, 1975, Topography of the south Pacific, *IMR Tech. Rep. Series TR56, Scripps Inst. of Oceanography.*

OKAMOTO, T. and T. MIYATAKE, 1989, Effects of near source seafloor topography of long-period teleseismic P waveforms, *Geophys. Res. Lett.*, **16**, 1309–1312.

PARSONS, B. and F. M. RICHTER, 1980, A relation between the driving force and geoid anomaly associated with mid-oceanic ridges, *Earth Planet. Sci. Lett.*, **51**, 445–450.

RUFF, L. J. and H. KANAMORI, 1983, The rupture process and asperity distribution of

three great earthquakes from long-period diffracted P-waves, *Phys. Earth Planet. Irter.*, **31**, 202-230.

SENO, T., S. HONDA and E. PETERSON, 1990, Depth of large outer-rise earthquakes and their implications for the rheology of the oceanic lithosphere, in preparation.

STEIN, S. and D. A. WIENS, 1986, Depth determination for shallow teleseismic earthquakes: Method and results, *Rev. Geophys.*, **24**, 806-832.

WARD, S. N., 1983, Body wave inversion; moment tensors and depths of oceanic intraplate bending earthquakes, *J. Geophys. Res.*, **88**, 9315-9330.

WIENS, D. A., 1987, Effects of near source bathymetry on teleseismic P waveforms, *Geophys, Res. Lett.*, **14**, 761-764.

WIENS, D. A. and S. STEIN, 1985, Implications of oceanic intraplate seismicity for plate stresses, driving forces and rheology, *Tectonophysics*, **116**, 143-162.

1981年10月16日チリ地震の深さの解析

地震研究所　瀬野徹三
広島大学理学部　本多了

浅い大地震の断層の深さ方向の広がりを推定する方法を提案した．この方法では，有限の広がりは，深さ方向に等間隔で置かれた点震源の重ね合わせで表現される．これらの点震源は同じメカニズムを持ち，速度 3 km/sec で上，あるいは下方向に伝播するものとした．様々な断層の拡がりに対しグリーン関数を計算し，それらを用いて観測波形の deconvolution を行い，震源時間関数を求める．観測波形と合成波形の残差が最小となる深さの拡がりを解とする．

合成波形をデータとして用い，その合成に用いられたものと異なるグリーン関数を用いて deconvolution を行う実験により，仮定された破壊伝播速度，地殻構造，海水層の厚さ，メカニズム解の，deconvolution の結果に与える影響を見積もった．結果は，破壊伝播速度にはほとんど左右されないが，地殻構造，特に海水層の厚さには大きく影響される．メカニズムの影響も無視出来ない．

我々はこの方法を1981年10月16日チリ地震 (M_S=7.2) に適用した．この地震はチリ海溝の outer-rise で起きた東西圧縮の地震である．海水層の厚さは残差・震源時間関数の振舞いから 4.5 km と見積もった．10 km 間隔の点震源を用いて観測波形を deconvolution することにより，30ないし 40 km の点震源あるいは 30-40 km の深さの拡がりが得られた．さらに，色々な深さの拡がりを仮定して合成された波形を deconvolution し，それを観測波形を deconvolution した結果と比較することにより，最適解として，深さの中心 35 km，拡がり 12 km (±3 km)，下から上への伝播を求めた．

この深さは，チリ沖で沈み込むプレートの曲げに伴う応力の中立面が，チリ地震の際特に上下しなかったことを示しており，プレートの曲げに伴う応力がテクトニックな応力より大きいことを意味する．